Effects of electron-impurity scattering on density of states in silicene: Impurity bands and band-gap narrowing

S. Y. Liu,* Y. C. Zeng, and X. L. Lei

Key Laboratory of Artificial Structures and Quantum Control (Ministry of Education), Department of Physics and Astronomy, Shanghai Jiao Tong University, 800 Dongchuan Road, Shanghai 200240, China

and Collaborative Innovation Center of Advanced Microstructures, Nanjing 210093, China

(Received 16 September 2016; published 29 December 2016)

Considering the interband correlation, we present a generalized multiple-scattering approach of Green's function to investigate the effects of electron-impurity scattering on the density of states in silicene at zero temperature. The reduction of energy gaps in the case of relatively high chemical potential and the transformation of split-off impurity bands into band tails for low chemical potential are found. The dependency of optical conductivity on the impurity concentration is also discussed for frequency within the terahertz regime.

DOI: 10.1103/PhysRevB.94.235308

I. INTRODUCTION

Recently, silicene, a single layer of silicon atoms, has attracted a great deal of experimental and theoretical interest [1–39]. This two-dimensional system has a hexagonal honeycomb structure, similar to the graphene, but with a periodically buckled topology. Due to the strong intrinsic spin-orbit coupling (SOC), the energy gaps of silicene near Dirac cones are relatively larger than those in graphene. The magnitude of the energy gap due to intrinsic SOC may reach a value of about $2\Delta_{SO} = 1.55 \sim 7.9$ meV (Δ_{SO} is the characteristic energy of this SOC) [7,8]. Besides, the specific buckled structure enables us to control the energy gap of silicene by applying an external perpendicular electric field [11,12,15,24]. These properties make the silicene a promising candidate for future electronic and spintronic applications. In experiment, silicene has been successfully fabricated via epitaxial growth on the Ag(111) [5,9,16,19,20], ZrB_2(0001) [10], ZrC(111) [27], Ir(111) [25], and MoS_2 surfaces [28] and the silicene field effect transistor (FET) operating at room temperature has also been realized very recently [32]. In theory, many interesting phenomena in silicene, such as the phase transition from a quantum spin-Hall state to a trivial insulating state [7,13,14,21–23,26], the intrinsic spin-Hall and valley-Hall effects induced by ac and dc electric fields [23,26,31], etc., have been predicted.

The magnitudes of energy gaps in a material play the key role in electronic device designing and development. They are also essential for the observation of many fundamental effects in condensed matter physics, such as quantum spin-Hall effect, quantum anomalous Hall effect, etc. However, previous studies in bulk semiconductors indicated that impurities may strongly affect the energy gaps in the material [40]. When the concentration of impurities is relatively dilute, electron-impurity scattering may introduce discrete energy levels within energy gaps. However, as the impurity density increases, additional bands may form inside or/and outside of the energy gaps. These impurity bands (IBs) are further transformed into the band tails in highly doped semiconductors, leading to the reduction of energy gaps. Similar phenomena were also shown in conventional two-dimensional electron gases [41–43]: when the density of impurities increases, the width of split-off impurity band increases and the IB is finally transformed into the band tail. The dependency of band tailing on the dopant concentration in heavily n-type doped superlattices and single wells was also studied [44,45]. However, it remains unclear how the electron-impurity scattering affects the energy gaps in new-type two-dimensional (2D) systems such as graphene, silicene, and germanene, etc., where the band gaps are relatively small and the scattering may lead to strong interband correlation, which plays a substantial role in the study of electronic states.

To investigate the impurity problems in conventional bulk and low-dimensional semiconductors, many theoretical approaches have been proposed, including coherent-potential approximation [46], path-integral approach [42–44,47–49], semiclassical models [50–52], instanton method [53], multiple-scattering approach (MSA) [41,45,54,55], etc. Among these, MSA, a Green's function (GF) method within multiple-scattering approximation, enables to correctly describe the evolution of electronic band structure with the doping concentration. In present paper, we generalize the MSA in the presence of the interband coherence and present a theoretical study of the effects of electron-impurity scattering on the density of states (DOS) and optical conductivity in silicene. The dependencies of DOS on the impurity density at various chemical potentials are carried out. The optical conductivities versus frequency within terahertz regime for various impurity densities are discussed.

The paper is organized as follows. In Sec. II, we present the Green's function approach within the multiple-scattering approximation in the presence of interband correlation. The numerical results are shown in Sec. III. Finally, we conclude our results in Sec. IV and append the derivation of the multiple-band Kubo formula in Appendix.

II. THEORETICAL FORMULATION

A two-dimensional massive Dirac fermion with momentum $\mathbf{k} \equiv (k_x, k_y)$ and electric charge $-e$ near the K or K' Dirac node in buckled silicene is described by a Hamiltonian of the form

*liusy@sjtu.edu.cn

$[\lambda_{\eta\sigma} = \Delta_z - \eta\sigma\Delta_{\rm SO}]$

$$\check{h}_{\eta\sigma}(\mathbf{k}) = v_F(\eta k_x\hat{\tau}_x + k_y\hat{\tau}_y) + \lambda_{\eta\sigma}\hat{\tau}_z, \tag{1}$$

where $\eta = \pm 1$ is the valley index for K and K', $\sigma = \pm 1$ is the spin index for spin up and down, $\hat{\tau}_i$ $(i = x,y,z)$ represent the Pauli matrices, and $v_F \approx 5.0 \times 10^5$ m/s is the Fermi velocity of Dirac fermions in silicene. There exist two types of SOC in silicene: the intrinsic SOC with characteristic energy about $\Delta_{\rm SO} \approx 3.9$ meV [8,15] and the SOC induced by the hybridization of p_z orbitals with σ orbitals of silicon atoms. The last one, which is described by an energy Δ_z, can be tuned by applying an external electric field along z direction [11].

Hamiltonian (1) in pseudo-spin basis can be diagonized: it reduces to a diagonal pseudo-helicity-basis Hamiltonian of the form $\hat{h}_{\eta\sigma}(\mathbf{k}) = {\rm diag}[\varepsilon_{\eta\sigma,+}(k),\varepsilon_{\eta\sigma,-}(k)]$ with $\varepsilon_{\eta\sigma\mu}(k) = \mu g_{\eta\sigma;k}$, $g_{\eta\sigma;k} \equiv \sqrt{v_F^2k^2 + \lambda_{\eta\sigma}^2}$, and $\mu = \pm$ as the helicity index. Correspondingly, the left- and right-helicity wave functions, $\Psi_{\eta\sigma\mu\mathbf{k}}(\mathbf{r})$, take the forms $\Psi_{\eta\sigma\mu\mathbf{k}}(\mathbf{r}) = \psi_{\eta\sigma\mu}(\mathbf{k})e^{i\mathbf{k}\cdot\mathbf{r}}$ with $\psi_{\eta\sigma\mu}(\mathbf{k})$ given by

$$\psi_{\eta\sigma\mu}(\mathbf{k}) = \frac{1}{\sqrt{2g_{\eta\sigma;k}(g_{\eta\sigma;k} - \mu\lambda_{\eta\sigma})}}\begin{pmatrix}\eta\mu v_F k e^{-i\eta\varphi_{\mathbf{k}}}\\ g_{\eta\sigma;k} - \mu\lambda_{\eta\sigma}\end{pmatrix}. \tag{2}$$

Here, k and $\varphi_{\mathbf{k}}$ are the magnitude and angle of momentum $\mathbf{k}$, respectively.

The sketches of $\varepsilon_{\eta\sigma\mu}(\mathbf{k})$ and of the DOSs of electrons in the pure system are given in Fig. 1. It is clear that for Hamiltonian (1) there are four bands near each Dirac node, corresponding to the cases $\sigma = \pm 1$ and $\eta = \pm 1$. The values of energy gaps are $2|\Delta_z - \Delta_{\rm SO}|$ and $2(\Delta_z + \Delta_{\rm SO})$ for spin-up (spin-down) and spin-down (spin-up) bands near the K (K') node, respectively. The carriers near one Dirac node are spin polarized, but the system remains paramagnetic since spins of electrons near K and K' are polarized in opposite directions. From Fig. 1(b), we also see that, in the pure silicene system, the DOSs of electrons linearly depend on E when E lies outside the energy gaps.

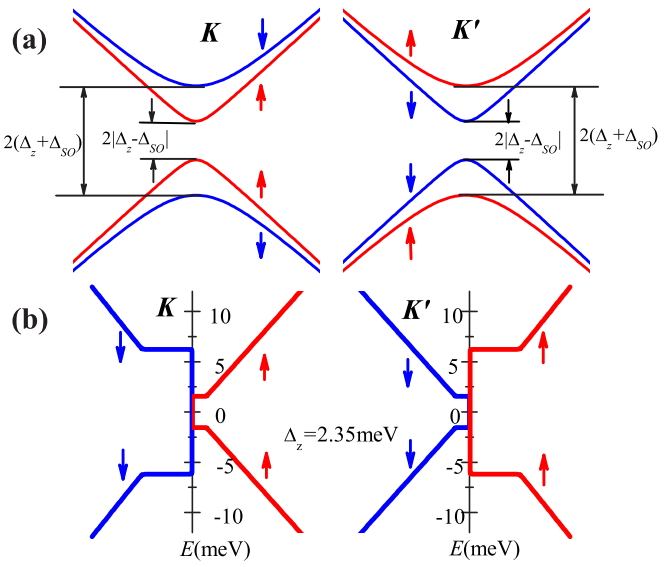

FIG. 1. Sketches of (a) the dispersion relations and (b) densities of states of spin-up and spin-down electrons near Dirac nodes in pure silicene for $\Delta_z = 2.35$ meV. The arrows in (a) and (b) indicate the directions of electron spins.

In realistic systems, the DOSs near the minima or maxima of bands strongly depend on the electron-impurity scattering, which is usually described by a potential $V(\mathbf{q})$ in the pseudo-spin basis. In pseudo-helicity basis, the scattering potential takes the form, $\hat{V}_{\eta\sigma;\mu\nu}(\mathbf{k},\mathbf{k}') = \psi^+_{\eta\sigma\mu}(\mathbf{k})V(\mathbf{k}-\mathbf{k}')\psi_{\eta\sigma\nu}(\mathbf{k}')$, corresponding to scattering of an electron in the valley η with spin σ from state $(\nu,\mathbf{k}')$ to state $(\mu,\mathbf{k})$ by impurities.

Further, we employ a Green's function approach to carry out the effects of electron-impurity interaction on the density of states and optical conductivity in silicene. The previous studies of impurity problems in one-band models indicated that [41,45,54,55] to correctly describe the split-off impurity bands and the band tails, GF should be considered within the multiple-scatting approximation, first proposed by Klauder [56]. On the other hand, in silicene, the interband correlation induced by electron-impurity scattering is quite important: it leads to residual conductivity when the density of carriers in silicene essentially vanishes [31]. Hence, to evaluate the Green's function, generalizing the one-band multiple-scattering method to the two-band case with consideration of interband correlation is required.

In pseudohelicity basis, the noninteracting retarded Green's function of an electron in valley η with spin σ, $\hat{g}^r_{\eta\sigma;\mu\nu}(\mathbf{k},E)$, takes a diagonal form (δ is an infinitesimal parameter)

$$\hat{g}^r_{\eta\sigma;\mu\nu}(\mathbf{k},E) = \frac{\delta_{\mu\nu}}{E - \varepsilon_{\eta\sigma;\mu}(\mathbf{k}) + i\delta}, \tag{3}$$

while the perturbative Green's function, $\hat{G}^r_{\eta\sigma;\mu\nu}(\mathbf{k},E)$, relates to the self-energy, $\hat{\Sigma}^r_{\eta\sigma;\mu\mu_1}(\mathbf{k},E)$, via the Dyson's equation of the form

$$\hat{G}^r_{\eta\sigma;\mu\nu}(\mathbf{k},E) = \hat{g}^r_{\eta\sigma;\mu\mu}(\mathbf{k},E)\delta_{\mu\nu} + \hat{g}^r_{\eta\sigma;\mu\mu}(\mathbf{k},E) \times \sum_{\mu_1}\hat{\Sigma}^r_{\eta\sigma;\mu\mu_1}(\mathbf{k},E)\hat{G}^r_{\eta\sigma;\mu_1\nu}(\mathbf{k},E). \tag{4}$$

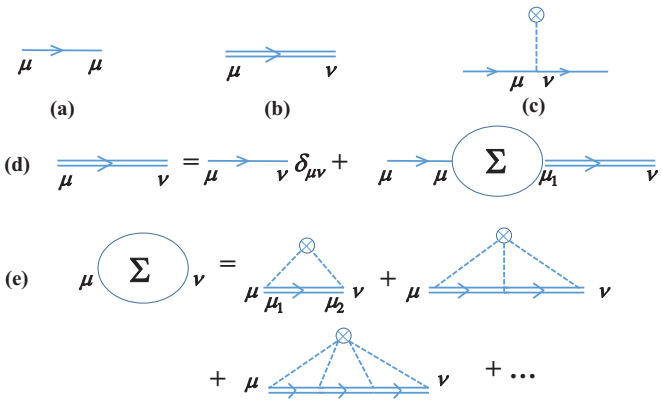

FIG. 2. Feynman diagrams for evaluation of retarded Green's function within multiple-scattering approximation. (a), (b), and (c) show the noninteracting retarded GF, perturbative retarded GF, and the vertex of electron-impurity scattering, respectively. (d) The Dyson's equation and (e) the Feynman diagram of self-energy within multiple-scattering approximation. Here, the indices η and σ are dropped for brevity.

In the multiple-scattering approach, $\hat{\Sigma}^r_{\eta\sigma;\mu\mu_1}(\mathbf{k},E)$ is determined by the Feynman diagrams presented in Fig. 2. It can be written as

$$\begin{aligned}\hat{\Sigma}^r_{\eta\sigma;\mu\nu}(\mathbf{k},E) = n_i \sum_{\mathbf{q}',\mu_1\mu_2} & \hat{V}_{\eta\sigma;\mu\mu_1}(\mathbf{k},\mathbf{q}')\hat{G}^r_{\eta\sigma;\mu_1\mu_2}(\mathbf{q}',E) \\ & \times \hat{V}_{\eta\sigma;\mu_2\nu}(\mathbf{q}',\mathbf{k}) \\ & + n_i \sum_{\substack{\mathbf{q}',\mathbf{q}'' \\ \mu_1\mu_2\mu_3\mu_4}} \hat{V}_{\eta\sigma;\mu\mu_1}(\mathbf{k},\mathbf{q}')\hat{G}^r_{\eta\sigma;\mu_1\mu_2}(\mathbf{q}',E) \\ & \times \hat{V}_{\eta\sigma;\mu_2\mu_3}(\mathbf{q}',\mathbf{q}'')\hat{G}^r_{\eta\sigma;\mu_3\mu_4}(\mathbf{q}'',E) \\ & \times \hat{V}_{\eta\sigma;\mu_4\nu}(\mathbf{q}'',\mathbf{k}) + \ldots \end{aligned} \tag{5}$$

with n_i as the impurity density. Further, we introduce a vertex function, $\hat{K}_{\eta\sigma;\mu\nu}(\mathbf{k},\mathbf{q};E)$, which satisfies the equation

$$\begin{aligned}\hat{K}_{\eta\sigma;\mu\nu}(\mathbf{k},\mathbf{q};E) = \sum_{\mathbf{q}',\mu_1\mu_2} & \hat{V}_{\eta\sigma;\mu\mu_1}(\mathbf{q},\mathbf{q}')\hat{G}^r_{\eta\sigma;\mu_1\mu_2}(\mathbf{q}',E) \\ & \times \left[n_i \hat{V}_{\eta\sigma;\mu_2\nu}(\mathbf{q}',\mathbf{k}) + \hat{K}_{\eta\sigma;\mu_2\nu}(\mathbf{k},\mathbf{q}';E)\right]. \end{aligned} \tag{6}$$

Thus we have $\hat{\Sigma}^r_{\eta\sigma;\mu\nu}(\mathbf{k},E) = \hat{K}_{\eta\sigma;\mu\nu}(\mathbf{k},\mathbf{q}=\mathbf{k};E)$.

To solve Eqs. (4) and (6) in a self-consistent manner, we express the perturbative retarded Green's function in terms of Fourier series, $\hat{G}^r_{\eta\sigma}(\mathbf{k},\omega) = \sum_{n=0}^{\infty} \hat{G}^{c;nk}_{\eta\sigma}(\omega)\cos n\varphi_{\mathbf{k}} + \sum_{n=0}^{\infty} \hat{G}^{s;nk}_{\eta\sigma}(\omega)\sin n\varphi_{\mathbf{k}}$, and apply the iteration scheme proposed by Ng [57]. Whence $\hat{G}^r_{\eta\sigma}(\mathbf{k},\omega)$ is carried out, the density of states of electrons with spin σ near node η, defined as $D_{\eta\sigma}(\omega) = \sum_{\mathbf{k},\mu} \hat{G}^r_{\eta\sigma;\mu\mu}(\mathbf{k},\omega)$, can be obtained directly from the zeroth term of cosine Fourier series: $D_{\eta\sigma}(\omega) = \sum_{\mathbf{k},\mu} \hat{G}^{c;0k}_{\eta\sigma;\mu\mu}(\omega)$.

In experiment, the frequency-dependent optical conductivity is a powerful probe to measure the electronic states in materials. Ignoring the influence of electronic states induced by electron-impurity scattering, the ac conductivity in silicene has been investigated by Vargiamidis *et al.* [26]. In Ref. [58], the optical properties beyond the usual Dirac-cone approximation in clean silicene were also studied by first-principles calculations. Considering the change of band structure due to defects, the optical conductivity in silicene has been studied recently [59]. In these studies, the Kubo formula based on the single-particle assumption was employed and the interband coherence was completely ignored. In the present paper, we generalize the Kubo formula in the presence of the interband correlation to investigate the optical conductivity in silicene (the detailed procedure of deriving the Kubo formula is presented in Appendix). Ignoring the vertex correction, the real part of zero-temperature longitudinal conductivity for electrons with spin σ near Dirac node η, $\mathrm{Re}\sigma_{\eta\sigma;xx}(\omega_0)$, takes the form

$$\begin{aligned}\mathrm{Re}\sigma_{\eta\sigma,xx}(\omega_0) = \frac{1}{\omega_0} \sum_{\substack{\mu,\nu \\ \mu_1,\nu_1,\mathbf{k}}} \int_{\mu_0-\omega_0}^{\mu_0} \frac{d\omega_1}{2\pi} \Big\{ & \mathrm{Re}\big[\hat{j}^x_{\eta\sigma;\nu_1\mu}(\mathbf{k})\hat{j}^x_{\eta\sigma;\mu_1\nu}(\mathbf{k}) + \hat{j}^x_{\eta\sigma;\nu\mu}(\mathbf{k})\hat{j}^x_{\eta\sigma;\mu_1\nu_1}(\mathbf{k})\big]\big[\mathrm{Im}\hat{G}^{c;0k}_{\eta\sigma;\mu\mu_1}\mathrm{Im}G^{c;0k}_{\eta\sigma;\nu_1\nu}\big]_{\omega_1+\omega_0,\omega_1} \\ & \mathrm{Re}\big[\hat{j}^x_{\eta\sigma;\nu_1\mu}(\mathbf{k})\hat{j}^x_{\eta\sigma;\mu_1\nu}(\mathbf{k}) - \hat{j}^x_{\eta\sigma;\nu\mu}(\mathbf{k})\hat{j}^x_{\eta\sigma;\mu_1\nu_1}(\mathbf{k})\big]\big[\mathrm{Re}\hat{G}^{c;0k}_{\eta\sigma;\mu\mu_1}\mathrm{Re}G^{c;0k}_{\eta\sigma;\nu_1\nu}\big]_{\omega_1+\omega_0,\omega_1}\Big\}. \end{aligned} \tag{7}$$

Here, μ_0 is the chemical potential. $\hat{j}^i_{\eta\sigma;\mu\nu}(\mathbf{k})$ are the elements of the ith ($i = x,\ y$) component of the single-particle current in the pseudohelicity basis, which take the forms $\hat{j}^i_{\eta\sigma;\mu\nu}(\mathbf{k}) = -ev_F\psi^+_{\eta\sigma\mu}(\mathbf{k})(\frac{\partial\check{h}_{\eta\sigma}(\mathbf{k})}{\partial k_i})_{\mu\nu}\psi_{\eta\sigma\nu}(\mathbf{k})$. To derive Eq. (7), we assume that the dominant contribution to the current comes from the zeroth-order term of the Fourier series of $\hat{G}^r$ and the contribution associated with higher-order terms is ignored.

Note that in the present paper, we concentrate on the optical conductivity at zero temperature. Thus the Fermi function $n_F(\omega)$ reduces to the Heaviside step function $\theta(\mu_0-\omega)$ and thus the ω integration in Eq. (7) runs from $\mu_0-\omega_0$ to μ_0. If one has to evaluate the real part of optical conductivity at finite temperature, Eq. (A5) should be used and the ω integration running from $-\infty$ to $+\infty$ should be taken.

III. NUMERICAL RESULTS

Further, we present a numerical calculation to investigate the effects of electron-impurity interaction on the density of states and on the optical conductivity in silicene at zero temperature. In the calculation, the characteristic energy of SO coupling due to external electric field is chosen as $\Delta_z = 2.35$ meV. We assume that the main contribution to the self-energy of electrons comes from a screened scattering potential due to charged impurities: $V(q) = e^2/[2\kappa\epsilon_0 q\epsilon(q)]$. Here, κ is the dielectric constant of the substrate. In numerical calculations, $\kappa = 1$ is used for simplicity. If the effect of the substrate on electron-impurity scattering is considered, the values of n_i, presented in this paper, essentially correspond to the values of n_i/κ^2. $\epsilon(q) = 1 - v(q)\Pi(q)$ is the static dielectric function and $\Pi(q)$ is the static polarization function. At zero temperature, it takes the form [60–67]

$$\Pi(q) = -\frac{\mu_0}{2\pi v_F^2}\sum_{\sigma,\eta}[F(q)\theta(|\lambda_{\eta\sigma}|-\mu_0)+G(q)\theta(\mu_0-|\lambda_{\eta\sigma}|)],$$

$F(q)$ and $G(q)$, respectively, take the forms [$k_F^{\eta\sigma} = \sqrt{\mu_0^2-\lambda_{\eta\sigma}^2}$]

$$F(q) = \frac{|\lambda_{\eta\sigma}|}{2\mu_0} + \frac{v_F^2q^2-4\lambda_{\eta\sigma}^2}{4v_Fq\mu_0}\arcsin\left(\sqrt{\frac{v_F^2q^2}{v_F^2q^2+4\lambda_{\eta\sigma}^2}}\right) \tag{8}$$

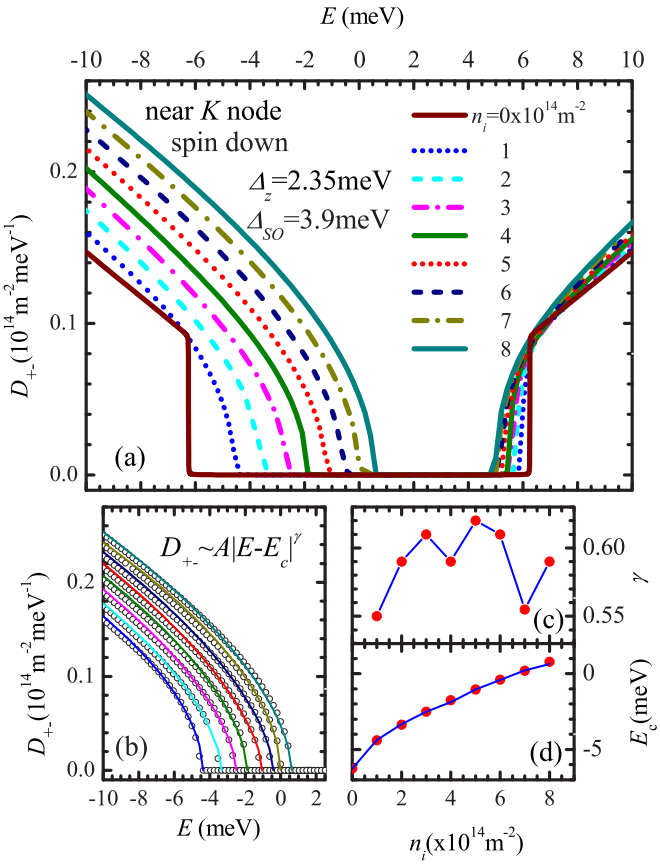

FIG. 3. (a) Densities of states of spin-down electrons in silicene for various impurity densities near the Dirac point K. The chemical potential is $\mu_0 = 20$ meV and the energy due to the SO coupling induced by the external electric field is $\Delta_z = 2.35$ meV. (b) Fitting of DOSs near the top of the lower band in (a) by the power-law formula $D_\pm = A|E - E_c|^\gamma$. The data from (a) are shown by open circles and the solid lines are the best fit lines of these data. From bottom to top, the impurity densities are $n_i = 1$, 2, 3, 4, 5, 6, 7, and 8×10^{14} m^{-2}. The dependencies of the fitting parameters γ and E_c on impurity densities are shown by filled circles in (c) and (d), respectively. The solid line in (d) is the best fit line of data: $\frac{E_c}{\text{meV}} = -5.95 + 1.4(\frac{n_i}{10^{14}\text{m}^{-2}})^{0.75}$.

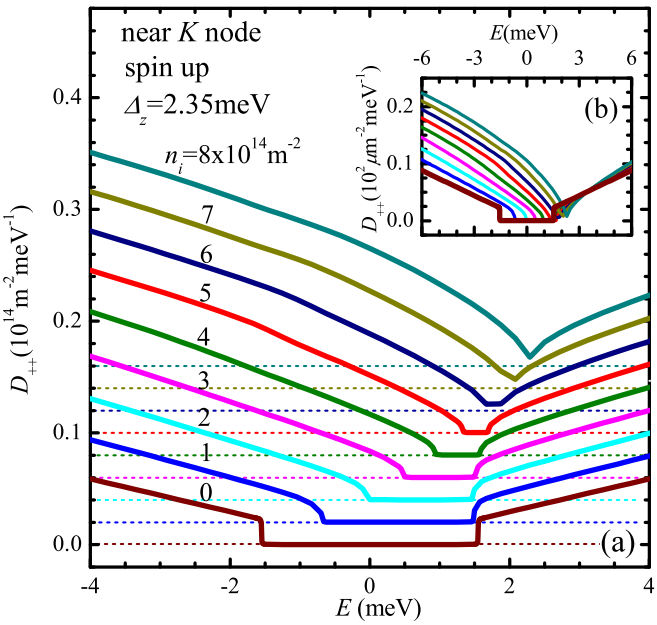

FIG. 4. (a) Densities of states of spin-up electrons in silicene for various impurity densities near the K node. For a guide to the eyes, each curve moves towards the upper side by $\Delta D_{++} = 2 \times 10^{12}$ m^{-2}meV^{-1} in sequence and the positions of $D_{++} = 0$ are indicated by horizontal dashed lines. (b) The same D_{xx} vs E as in (a) but without ΔD_{++} shift.

and

$$G(q) = 1 - \theta\left(q - 2k_F^{\eta\sigma}\right)\left[\frac{\sqrt{q^2 - 4\left(k_F^{\eta\sigma}\right)^2}}{2q} - \frac{v_F^2 q^2 - 4\lambda_{\eta\sigma}^2}{4v_F q\mu_0}\arctan\left(\frac{\sqrt{v_F^2 q^2 - 4\left(k_F^{\eta\sigma}\right)^2 v_F^2}}{2\mu_0}\right)\right].$$

A. Split-off impurity bands and band-gap narrowing

We first analyze the effects of electron-impurity scattering on the density of states in silicene. It is well known that in conventional semiconductors, introduction of impurities produces local energy levels lying within the energy gap. These levels broaden into impurity bands when the concentration of impurities increases. Further, in heavily doped semiconductors, the impurity bands may be combined with a conduction or a valence band, forming a band tail and leading to band-gap narrowing. In conventional two-dimensional electron gases, the transition from the split-off impurity band at low impurity concentration to a band tail at high impurity concentration has also been demonstrated theoretically [41–43]. Hence similar phenomena are expected to be observed in silicene.

In Fig. 3(a), we plot the densities of states of electrons with spin down near the K node (i.e., $\sigma = -1$ and $\eta = 1$) for various impurity densities. The chemical potential is $\mu_0 = 20$ meV. It is clear that, when the impurity density increases, the energy gaps become narrower. In our study, a repulsive potential of electron-impurity scattering is considered and the impurities essentially play the role of acceptors. Hence band-gap narrowing mainly comes from the movement of the top of the lower energy band towards the high-energy side. However, remarkable shifts of the upper energy band bottom towards the low-energy side can also be observed due to strong band correlations in silicene.

Note that when $n_i = 0$, there are two discontinuities in $D_\pm$ versus E at $E = \pm|\Delta_{\text{SO}} - \Delta_z|$. In the presence of electron-impurity scattering, they are smeared out and $D_\pm$ continuously changes with E. Such $D_\pm$ versus E can be described by a power-law formula, $D_\pm \sim A|E - E_c|^\gamma$. In Fig. 3(b), we show the fitting of $D_\pm$ near the top of the lower energy band for various impurity densities. The parameters γ and E_c are assumed to be n_i dependent: γ and E_c versus n_i are given by Figs. 3(c) and 3(d), respectively. We find that the values of γ are in the range $0.5 \sim 0.65$ and the E_c versus n_i can be further fitted by $\frac{E_c}{\text{meV}} = -5.95 + 1.4(\frac{n_i}{10^{14}\text{m}^{-2}})^{0.75}$.

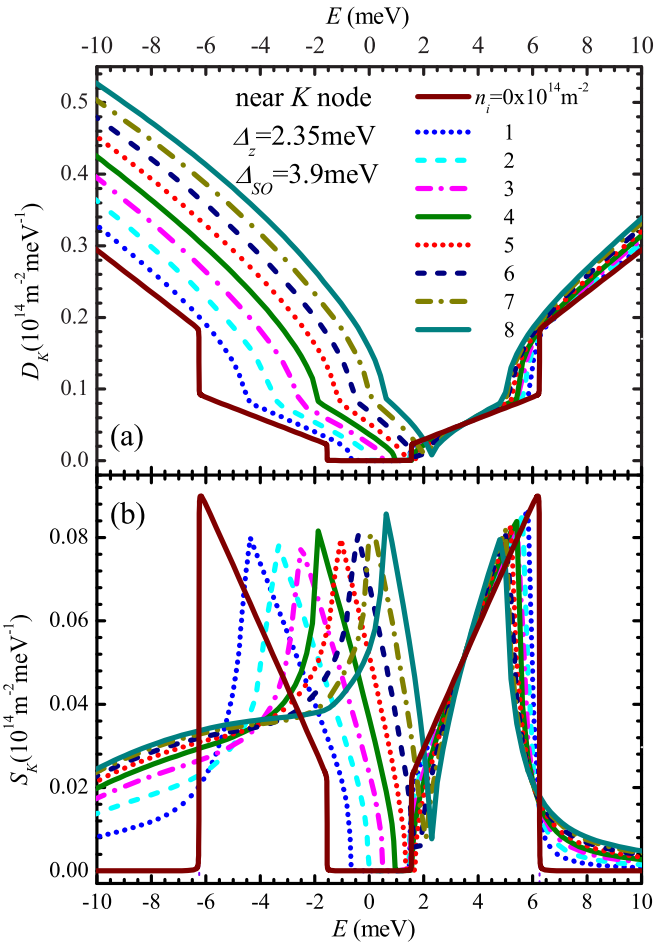

FIG. 5. Energy dependencies of (a) total DOSs, $D_K = D_{++} + D_{+-}$ and of (b) spin-polarized DOSs, $S_K = D_{++} - D_{+-}$ of electrons near the K node for various impurity densities. The other parameters are the same as in Fig. 3.

In Fig. 3, the spins of carriers near K node are assumed to be polarized in the down direction. Correspondingly, the energy gap is $2(\Delta_z + \Delta_{SO}) = 10.5$ meV, which is relatively large. Hence, in the case $n_i \leqslant 8 \times 10^{14}$ m^{-2}, the complete disappearance of energy gaps does not show up. However, for the spin-up electrons near K node, the energy gap becomes small: $2|\Delta_z - \Delta_{SO}| = 3.1$ meV and the vanishing of the energy gap is relatively easy to be seen. In Fig. 4, we plot the energy dependencies of the densities of states of electrons with spin up near the K node (i.e., $\eta = +$ and $\sigma = +$). It is clear that when the density of impurities increases from $n_i = 0$ but still remains relatively low, band-gap narrowing can be observed. However, when n_i further ascends, so that $n_i \gtrsim 5 \times 10^{14}$ m^{-2}, the energy gap disappears completely.

Further, in Fig. 5(a), we plot the energy dependencies of the total DOSs of electrons near the K node, $D_K = D_{++} + D_{+-}$, for various impurity densities. In the absence of electron-impurity scattering, four discontinuities in D_K versus E can be observed at $E = \pm|\Delta_{SO} \pm \Delta_z|$. In the presence of impurities, they are smeared out but "dog-leg" shaped connections still can be seen. When energy increases, D_K first decreases and then it may reach the zero value for $n_i \lesssim 5 \times 10^{14}$ m^{-2}, forming an energy gap. When E further increases, D_K also increases. For relatively high impurity density ($n_i \gtrsim 5 \times 10^{14}$ m^{-2}), D_K is always nonzero and the energy gap disappears completely.

One of the interesting properties in silicene is that the electrons near each Dirac node are spin polarized, although the net spin polarization of electrons vanishes. In Fig. 3(b), we show the energy dependencies of spin-polarized DOSs, defined as $S_\eta = D_{\eta+} - D_{\eta-}$, for various densities of impurities. We see that in pure silicene, S_K is nonzero only within the energy ranges $-|\Delta_{SO} + \Delta_z| < E < -|\Delta_{SO} - \Delta_z|$ (denoted as range I) and $|\Delta_{SO} - \Delta_z| < E < |\Delta_{SO} + \Delta_z|$ (denoted as range II). When E increases, S_K linearly decreases in range I while it linearly increases in range II. In the presence of electron-impurity scattering, the range of nonvanishing S_K becomes broader. In particular, when n_i increases, the range of vanishing S_K between $-|\Delta_{SO} - \Delta_z| < E < |\Delta_{SO} - \Delta_z|$ becomes narrower and finally disappears when $n_i \gtrsim 5 \times 10^{14}$ m^{-2}. Besides, S_K is also nonzero for $|E| > |\Delta_{SO} + \Delta_z|$ in the presence of impurities.

In Figs. 3–5, we do not observe the split-off impurity bands since in these cases the chemical potential is relatively large. To demonstrate the IBs, in Fig. 6, we plot the densities of states of electrons with spin-up near K node for various chemical potentials close to the upper limit of gap, $|\Delta_{SO} - \Delta_z| = 1.55$ meV: $\mu_0 = 1.58$, 1.59, 1.60, 1.61, 1.62, 1.63, 1.64, and 1.65 meV. The impurity concentration is assumed relatively low, $n_i = 1 \times 10^{10}$ m^{-2}. It is obvious that, for these chemical potentials, D_{++} are almost the same within the most part of

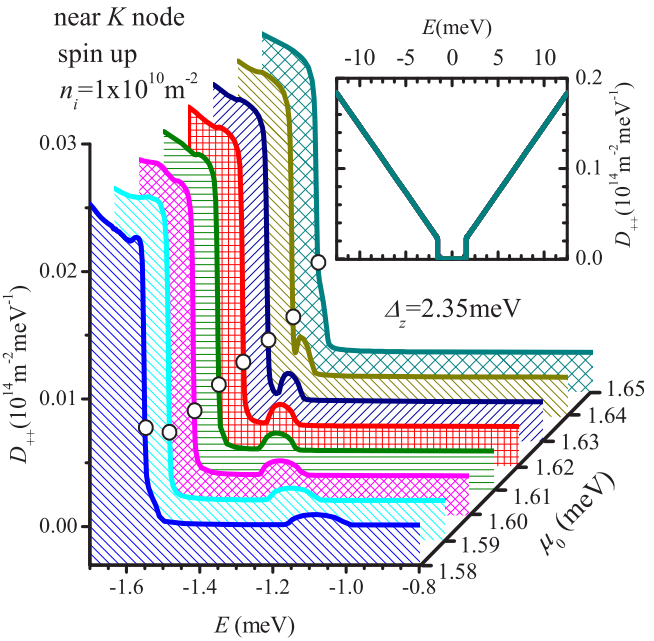

FIG. 6. DOSs of spin-up electrons near K node in silicene for various chemical potentials near the top of the lower energy band. The density of impurities is $n_i = 1 \times 10^{-10}$ m^{-2} and $\Delta_z = 2.35$ meV. From bottom to top, the chemical potentials are $\mu_0 = 1.58$, 1.59, 1.60, 1.61, 1.62, 1.63, 1.64, and 1.65 meV, correspondingly. The circles on curves indicate the DOSs at energy $E = -1.55$ meV, which corresponds to the lower limit of energy gap for electrons with $\eta = \sigma = +1$ in the pure system. The inset shows D_{++} versus E for various chemical potentials within an enlarged energy scale.

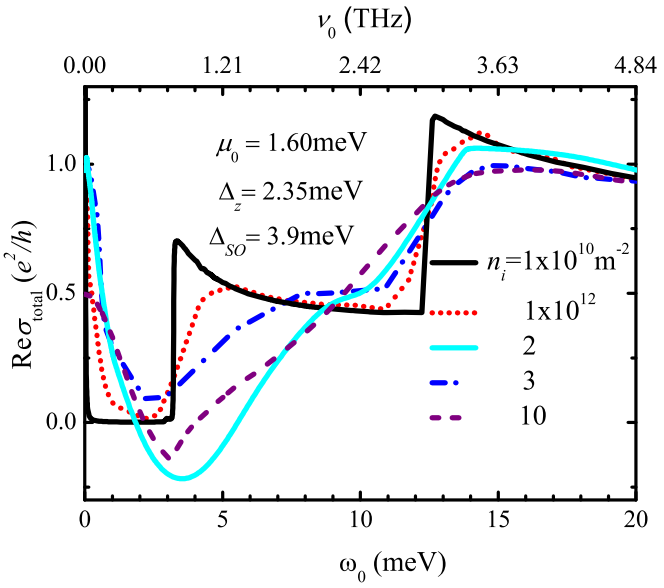

FIG. 7. The frequency dependencies of real part of total optical conductivity in silicene for various impurity densities $n_i = 1 \times 10^{10}$, 1×10^{12}, 2×10^{12}, 3×10^{12}, and 1×10^{13} m^{-2}. The chemical potential is $\mu_0 = 1.60$ meV, $\Delta_z = 2.35$ meV, and $\Delta_{SO} = 3.9$ meV.

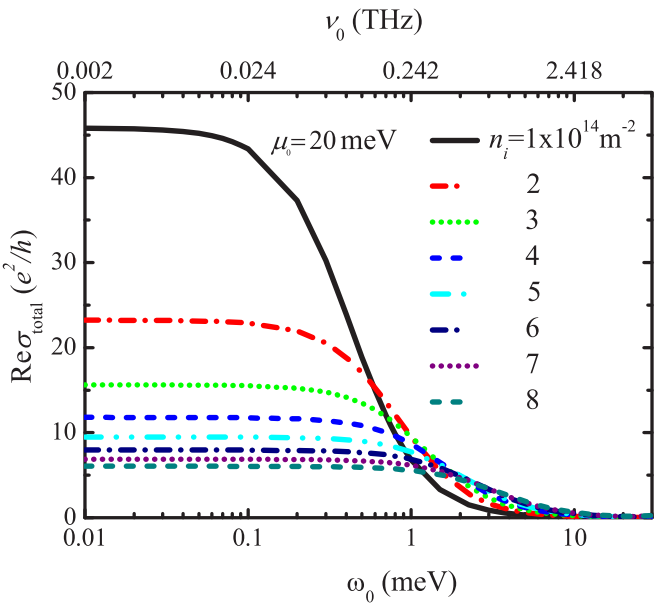

FIG. 8. Reσ_{total} vs ω_0 (or ν_0) for various impurity densities $n_i = 1$, 2, 3, 4, 5, 6, 7, 8×10^{14} m^{-2}. The chemical potential is $\mu_0 = 20$ meV. Other parameters are the same as those in Fig. 7.

energy range studied here (see the inset of Fig. 6), except for E near the top of lower energy band. We see that in the case of E close to -1.55 meV, i.e., the lower limit of energy gap in a pure silicene, impurity bands are formed for $\mu_0 = 1.58 \sim 1.64$ meV. When the chemical potential increases, the center of IB moves towards the low-energy side that it finally disappears and combines with the valence bands at $\mu_0 = 1.65$ meV.

B. Optical conductivity

After self-consistent evaluation of retarded Green's functions within the multiple-scattering approximation, the optical conductivity can be carried out by means of Eq. (7). The results are presented in Figs. 7 and 8.

In Fig. 7, we plot the real part of total optical conductivity, $\mathrm{Re}\sigma_{\mathrm{total}} \equiv \sum_{\eta,\sigma=\pm} \mathrm{Re}\sigma_{\eta\sigma,xx}(\omega_0)$, versus frequency ω_0 (or $\nu_0 = \omega_0/h$) for various impurity densities $n_i = 1 \times 10^{10}$, 1×10^{12}, 2×10^{12}, 3×10^{12}, and 1×10^{13} m^{-2}. The chemical potential is chosen to be $\mu_0 = 1.60$ meV, which is close to the upper limit of energy gap. When the impurity density is relatively small (in the case $n_i = 1 \times 10^{-10}$ m^{-2}), we can observe two peaks which correspond to the optical excitations of electrons from two branches of valence bands: when ω_0 increases from $\omega_0 < 2|\Delta_z \pm \Delta_{\mathrm{SO}}|$ (i.e., 3.1 and 6.5 meV) to $\omega_0 > 2|\Delta_z \pm \Delta_{\mathrm{SO}}|$, Re$\sigma_{\mathrm{total}}$ first abruptly increases and then gradually decreases. When the impurity density increases and reaches the value of order of 1×10^{12} m^{-2}, two peaks begin to be smeared out due to the increase of DOS within the energy gap. The peak near $\omega_0 = 6.5$ meV reduces monotonically when n_i ascends. However, near the lower frequency location ($\omega_0 = 2|\Delta_z - \Delta_{\mathrm{SO}}| = 3.1$ meV) the peak first decreases rapidly when n_i increases and then disappears completely at $n_i = 2 \times 10^{12}$ m^{-2}. When n_i further ascends, the dependence of Reσ_{total} on n_i for ω_0 becomes nonmonotonic: Reσ_{total} first increases with increasing n_i from 2 to 5×10^{12} m^{-2} and then decreases with further increase of n_i.

In Fig. 8, we plot the frequency dependencies of real part of total optical conductivity for the chemical potential $\mu_0 = 20$ meV, which corresponds to a metallic phase of silicene. When the frequency increases, Reσ_{total} decreases monotonically. The dependencies of the real part of optical conductivity on the impurity density are quite distinct for high and low optical frequencies: when n_i increases, Reσ_{total} decreases for $\omega_0 < 0.5$ meV, while it increases in the case $\omega_0 > 2.5$ meV.

From Figs. 7 and 8, it is clear that, to observe band-gap narrowing in the optical conductivity versus frequency, the chemical potential of silicene samples should be close to the energy gap and the concentration of impurities should be relatively low: n_i is of order of 10^{12} m^{-2}. Besides, we should also note that it is difficult to detect the split-off impurity bands from the optical conductivity study since the DOSs of impurity bands are much smaller than those out of energy gaps. To observe the IBs, more powerful experimental tools, such as angle-resolved photoemission spectroscopy (ARPES), pump-probe spectroscopy within terahertz regime, etc., are required.

IV. CONCLUSIONS

We have investigated the effects of electron-impurity scattering on the density of states and on the optical conductivity in silicene at zero temperature by using the multiple-scattering approach of Green's functions, generalized to include the interband correlation. We find that, in the case of relatively high chemical potential μ_0, the energy gap reduces with an increase of impurity density and it finally disappears when n_i reaches the magnitude of order of $\sim 5 \times 10^{14}$ m^{-2}. The split-off impurity bands can be observed only for low μ_0

and low n_i. They transform into band tails as μ_0 (or n_i) increases. We also find that, in the frequency dependence of the real part of conductivity for low n_i and low μ_0, there are two peaks associated with the interband excitations of electrons. These peaks are smeared out when the impurity density ascends. In the case of high μ_0, Reσ_{xx} versus n_i shows distinct behaviors for low and high frequency ω_0: as the impurity density increases, Reσ_{xx} decreases for low ω_0 while it increases in the case of high ω_0.

It should be noted that the isolated energy bands and the energy-gap narrowing in the DOS of electrons as well as the peak smearing in optical conductivity, predicted above, still can be observed if the value of Δ_z differing from that used in our numerical calculation. In a realistic system, Δ_z essentially depends on the substrates and on the external electric field applied perpendicular to the silicene plane. The change of Δ_z leads to a variation of the energy gaps $|\Delta_{SO} \pm \Delta_z|$. Correspondingly, the critical values of impurity density for observing the disappearance of the energy gap in DOS and the peak positions in the frequency dependence of optical conductivity change.

ACKNOWLEDGMENTS

This work was supported by the project of National Key Basic Research Program of China (973 Program) (Grant No. 2012CB927403) and National Natural Science Foundation of China (Grant No. 11274227).

APPENDIX: GENERALIZED KUBO FORMULA IN THE PRESENCE OF INTERBAND CORRELATION

In the previous studies on linear multiband transport, the Kubo formula without the vertex corrections has been widely used to interpret the dc and ac conductivities. In the typical form of this formula, the effect of interband transition induced by external dc and/or ac electric fields is considered, but the interband correlation induced by electron-impurity scattering is ignored. However, the last one is quite important in the narrow-band semiconductors as well as in new-type two-dimensional systems, such as graphene, silicene, germanene, etc. To correctly describe the dc and ac transport properties in these systems, a generalized Kubo formula is required.

We consider an equilibrium system of carriers, which may be scattered by impurities, phonons, etc. The single-particle Hamiltonian in the absence of scatterings is denoted by $\hat{h}_0(\hat{\mathbf{p}})$ with $\hat{\mathbf{p}}$ as the carrier momentum operator. Further, we assume that the eigenfunctions of $\hat{h}_0(\hat{\mathbf{p}})$ are known: they are denoted by $\psi_i(\mathbf{r})$ with i as the index of eigenvalues E_i. In the framework of Green's function approach, the motion of such an equilibrium system can be determined by the GFs, $\hat{G}^{r,a,<}(\mathbf{r},t;\mathbf{r}',t')$, in which the scatterings of carriers due to impurities, phonons, etc., are embedded. In the basis of eigenfunctions ψ_i, they can be rewritten as

$$\hat{G}^{r,a,<}(\mathbf{r},t;\mathbf{r}',t') = \sum_{i,j} \hat{G}^{r,a,<}_{ij}(t,t')\psi_i(\mathbf{r})\psi^*_j(\mathbf{r}'),$$

where $\hat{G}^{r,a,<}_{ij}(t,t')$ are the GFs based on eigenfunctions of $\hat{h}_0$ and they essentially depend only on the difference of two times. Note that according to Kubo-Martin-Schwinger relations [68,69] $G^<$ relates to $G^{r,a}$ in the ω space by

$$\hat{G}^<_{ij}(\omega) = -n_F(\omega)\big[\hat{G}^r_{ij}(\omega) - \hat{G}^a_{ij}(\omega)\big],$$

with $n_F(\omega) = [\exp((\omega-\mu_0)/T)+1]^{-1}$ as the Fermi function.

Further, we assume that the system is driven by an external electric field $\mathbf{E}(t)$, described by the vector potential $\mathbf{A}(t)$. In the framework of minimum coupling, the single-particle non-interacting Hamiltonian takes the form $\hat{h}'_0 \equiv \hat{h}_0(\hat{\mathbf{p}} + e\mathbf{A}(t))$. Up to the first order of electric field, $\hat{h}'_0$ can be further rewritten as $\hat{h}'_0 \approx \hat{h}_0(\hat{\mathbf{p}}) + \delta\hat{h}_0$. Here, δh_0 is the perturbed part due to $\mathbf{E}(t)$ and takes the form $\delta\hat{h}_0 = -\hat{\mathbf{j}}_0(\mathbf{r})\cdot\mathbf{A}(t)$ with $\hat{\mathbf{j}}_0(\mathbf{r}) = -e\nabla_{\mathbf{p}}\hat{h}_0(\hat{\mathbf{p}})$. Thus, up to the first order of $\mathbf{A}(t)$, the lesser Green's function out of equilibrium, $\hat{\mathcal{G}}^<$, takes the form

$$\hat{\mathcal{G}}^<(\mathbf{r},t;\mathbf{r}',t') = \hat{G}^<(\mathbf{r},t;\mathbf{r}',t') - \frac{1}{2}\int d\mathbf{r}''\int dt\hat{G}(\mathbf{r},t;\mathbf{r}'',t'') \times \{\mathbf{A}(t'')\cdot[\overrightarrow{\hat{\mathbf{j}}_0}(\mathbf{r}'') + \overleftarrow{\hat{\mathbf{j}}^+_0}(\mathbf{r}'')]\}\hat{G}(\mathbf{r}'',t'';\mathbf{r}',t')]^<, \tag{A1}$$

where the symbol $\rightharpoonup$ or $\leftharpoonup$, standing over the operators, denotes the direction of action.

To evaluate the conductivity, one has to carry out the single-particle current operator, $\mathbf{j}$. From the definition of current, $\mathbf{j} = -e\frac{d\mathbf{r}}{dt}$, and the motion of equation of $\mathbf{r}$, it follows

$$\hat{\mathbf{j}}(\mathbf{r},t) = -ie[\hat{h}'_0,\mathbf{r}] \approx -e\nabla_{\mathbf{p}}\hat{h}_0(\mathbf{p}) - e^2[\mathbf{A}(t)\cdot\nabla_{\mathbf{p}}]\nabla_{\mathbf{p}}\hat{h}_0(\mathbf{p}). \tag{A2}$$

$\hat{\mathbf{j}}(\mathbf{r},t)$ can be further rewritten as $\hat{\mathbf{j}}(\mathbf{r},t) = \hat{\mathbf{j}}_0(\mathbf{r}) + \delta\hat{\mathbf{j}}(\mathbf{r},t)$, with $\delta\hat{\mathbf{j}}(\mathbf{r},t) \equiv -e^2[\mathbf{A}(t)\cdot\nabla_{\mathbf{p}}]\nabla_{\mathbf{p}}\hat{h}_0(\hat{\mathbf{p}})$. The macroscopic current that observed in experiments, $\mathbf{J}(\mathbf{r},t)$, is determined by $J(\mathbf{r}) = -i\lim_{\mathbf{r}'\to\mathbf{r}}\frac{1}{2}[\hat{\mathbf{j}}(\mathbf{r},t) + \hat{\mathbf{j}}^+(\mathbf{r}',t)]\mathcal{G}^<(\mathbf{r},t;\mathbf{r}',t)$. Substituting Eqs. (A1) and (A2) into $\mathbf{J}(\mathbf{r},t)$ and retaining the terms up to the first order of $\mathbf{E}(t)$, we get

$$\begin{aligned}\mathbf{J}(\mathbf{r},t) = &-\frac{i}{2}\lim_{\mathbf{r}'\to\mathbf{r}}[\delta\hat{\mathbf{j}}(\mathbf{r},t) + \delta\hat{\mathbf{j}}^+(\mathbf{r}',t)]\hat{G}^<(\mathbf{r},t;\mathbf{r}',t)\\ &+\frac{i}{4}\lim_{\mathbf{r}'\to\mathbf{r}}[\hat{\mathbf{j}}_0(\mathbf{r}) + \hat{\mathbf{j}}^+_0(\mathbf{r}')]\int d\mathbf{r}''\\ &\times\int dt''[\hat{G}(\mathbf{r},t;\mathbf{r}'',t'')\{\mathbf{A}(t'')\cdot[\overrightarrow{\hat{\mathbf{j}}_0}(\mathbf{r}'') + \overleftarrow{\hat{\mathbf{j}}^+_0}(\mathbf{r}'')]\}\\ &\times\hat{G}(\mathbf{r}'',t'';\mathbf{r}',t)]^<.\end{aligned} \tag{A3}$$

In terms of eigenfunction representation of $G^<$, $\mathbf{J}(\mathbf{r},t)$ can be further rewritten as

$$\begin{aligned}\mathbf{J}(\mathbf{r},t) = &-i\sum_{ij}\delta\mathbf{j}_{ij}(\mathbf{r},t)\hat{G}^<_{ji}(t,t)\\ &+i\sum_{iji_1j_1}\int dt''\mathbf{j}_{0ij}(\mathbf{r})\mathbf{j}_{0j_1i_1}[\hat{G}_{jj_1}(t,t'')\hat{G}_{i_1i}(t'',t)]^<,\end{aligned}$$

where $\mathbf{j}_{0ij}(\mathbf{r}) \equiv \frac{1}{2}\lim_{\mathbf{r}\to\mathbf{r}'}[\hat{\mathbf{j}}_0(\mathbf{r}) + \hat{\mathbf{j}}^+_0(\mathbf{r}')]\psi_j(\mathbf{r})\psi^*_i(\mathbf{r}')$ and $\hat{\mathbf{j}}_{0ij} = \int d\mathbf{r}\mathbf{j}_{0ij}(\mathbf{r})$ is the element of matrix $\hat{\mathbf{j}}_0$. $\delta\mathbf{j}_{ij}(\mathbf{r})$ is defined in the same manner as $\mathbf{j}_{0ij}(\mathbf{r})$ but with replacing $\hat{\mathbf{j}}(\mathbf{r},t)$ and $\hat{\mathbf{j}}^+(\mathbf{r}',t)$ by operators $\delta\hat{\mathbf{j}}(\mathbf{r})$ and $\delta\hat{\mathbf{j}}^+(\mathbf{r}')$, respectively. Performing Fourier transform, the observed current in $(\mathbf{q},\omega)$

space is given by

$$\mathbf{J}(\mathbf{q},\omega) = -i\sum_{ij}\delta\mathbf{j}_{ij}(\mathbf{q},\omega)\int\frac{d\omega'}{2\pi}\hat{G}^{<}_{ji}(\omega) + i\sum_{iji_1j_1}\int\frac{d\omega_1}{2\pi}\mathbf{j}_{0ij}(\mathbf{q})\mathbf{j}_{0j_1i_1}\left[\hat{G}_{jj_1}(\omega_1)\hat{G}_{i_1i}(\omega_1-\omega)\right]^{<}.$$

Setting $\mathbf{q}=0$ and using the relation $J_\alpha(\omega) = i\omega\sum_{\beta=x,y,z}\sigma_{\alpha\beta}A_\beta(\omega)$ ($\sigma_{\alpha\beta}$ is the conductivity) and Kubo-Martin-Schwinger relation $\hat{G}^{<} = n_F(\omega)[\hat{G}^a(\omega)-\hat{G}^r(\omega)]$, we finally arrive at

$$\begin{aligned}\sigma_{\alpha\beta}(\omega) = {}& \frac{ie^2}{\omega}\sum_{ij}\frac{\partial^2}{\partial p_\alpha\partial p_\beta}[\hat{h}_0(\mathbf{p})]_{ij}\int\frac{d\omega'}{2\pi}[-i\hat{G}^{<}_{ji}(\omega)] \\ & + \frac{1}{\omega}\sum_{iji_1j_1}\int\frac{d\omega_1}{2\pi}\hat{j}^{\alpha}_{0ij}\hat{j}^{\beta}_{0j_1i_1} \\ & \times\left\{n_F(\omega_1-\omega)\left[\hat{G}^r_{jj_1}\left(G^a_{i_1i}-G^r_{i_1i}\right)\right]_{\omega_1,\omega_1-\omega}\right. \\ & \left. + n_F(\omega_1)\left[\left(G^a_{jj_1}-G^r_{jj_1}\right)\hat{G}^a_{i_1i}\right]_{\omega_1,\omega_1-\omega}\right\}. \qquad \text{(A4)}\end{aligned}$$

In this equation, the first term is just the diamagnetic term. It reduces to $iN_ee^2/(m\omega)$ (N_e is the carrier density) for a one-band Hamiltonian $\hat{h}(\mathbf{p}) = \mathbf{p}^2/(2m)$ but it vanishes when the free-carrier Hamiltonian depends linearly on $\mathbf{p}$. This implies that the diamagnetic term in conductivity is absent in Dirac-fermion systems, such as the systems with carriers near the Dirac nodes of graphene, silicene, germanene, etc.

Note that Eq. (A4) contains momentum integrations, which are implicitly involved in the summations. Due to the specific momentum dependence of $\hat{\mathbf{j}}_0$, in Eq. (A4), only the sums of the terms associated with real parts of quantity $\hat{j}^{\alpha}_{0ij}\hat{j}^{\alpha}_{0j_1i_1}$ are nonvanishing. Thus the real part of diagonal conductivity $\mathrm{Re}\sigma_{\alpha\alpha}$ can be further rewritten in a compact form:

$$\begin{aligned}\mathrm{Re}\sigma_{\alpha\alpha} = {}& \frac{1}{\omega}\sum_{iji_1j_1}\int\frac{d\omega_1}{2\pi}[n_F(\omega_1)-n_F(\omega_1+\omega)] \\ & \times\left\{\mathrm{Re}\left(\hat{j}^{\alpha}_{0i_1j}\hat{j}^{\alpha}_{0j_1i}+\hat{j}^{\alpha}_{0ij}\hat{j}^{\alpha}_{0j_1i_1}\right)\mathrm{Im}G^r_{jj_1}(\omega_1+\omega)\right. \\ & \times\mathrm{Im}G^r_{i_1i}(\omega_1)+\mathrm{Re}\left(\hat{j}^{\alpha}_{0i_1j}\hat{j}^{\alpha}_{0j_1i}-\hat{j}^{\alpha}_{0ij}\hat{j}^{\alpha}_{0j_1i_1}\right) \\ & \left.\times\mathrm{Re}G^r_{jj_1}(\omega_1+\omega)\mathrm{Re}G^r_{i_1i}(\omega_1)\right\}. \qquad \text{(A5)}\end{aligned}$$

Here, $\hat{G}^r_{ij} = (\hat{G}^a_{ji})^*$ is used.

[1] G. G. Guzmán-Verri and L. C. Lew Yan Voon, Phys. Rev. B **76**, 075131 (2007).
[2] S. Cahangirov, M. Topsakal, E. Aktürk, H. Şahin, and S. Ciraci, Phys. Rev. Lett. **102**, 236804 (2009).
[3] S. Lebègue and O. Eriksson, Phys. Rev. B **79**, 115409 (2009).
[4] P. De Padova, C. Quaresima, C. Ottaviani, P. M. Sheverdyaeva, P. Moras, C. Carbone, D. Topwal, B. Olivieri, A. Kara, H. Oughaddou, B. Aufray, and G. Le Lay, Appl. Phys. Lett. **96**, 261905 (2010).
[5] B. Lalmi, H. Oughaddou, H. Enriquez, A. Kara, S. Vizzini, B. Ealet, and B. Aufray, Appl. Phys. Lett. **97**, 223109 (2010).
[6] P. De Padova, C. Quaresima, B. Olivieri, P. Perfetti, and G. Le Lay, Appl. Phys. Lett. **98**, 081909 (2011).
[7] C.-C. Liu, W. Feng, and Y. Yao, Phys. Rev. Lett. **107**, 076802 (2011).
[8] C.-C. Liu, H. Jiang, and Y. Yao, Phys. Rev. B **84**, 195430 (2011).
[9] P. Vogt, P. De Padova, C. Quaresima, J. Avila, E. Frantzeskakis, M. C. Asensio, A. Resta, B. Ealet, and G. Le Lay, Phys. Rev. Lett. **108**, 155501 (2012).
[10] A. Fleurence, R. Friedlein, T. Ozaki, H. Kawai, Y. Wang, and Y. Yamada-Takamura, Phys. Rev. Lett. **108**, 245501 (2012).
[11] Z. Ni, Q. Liu, K. Tang, J. Zheng, J. Zhou, R. Qin, Z. Gao, D. Yu, and J. Lu, Nano Lett. **12**, 113 (2012).
[12] N. D. Drummond, V. Zólyomi, and V. I. Fal'ko, Phys. Rev. B **85**, 075423 (2012).
[13] L. Stille, C. J. Tabert, and E. J. Nicol, Phys. Rev. B **86**, 195405 (2012).
[14] A. Dyrdał and J. Barnaś, Phys. Status Solidi RRL **6**, 340 (2012).
[15] M. Ezawa, New J. Phys. **14**, 033003 (2012).
[16] C.-L. Lin, R. Arafune, K. Kawahara, N. Tsukahara, E. Minamitani, Y. Kim, N. Takagi, and M. Kawai, Appl. Phys. Express **5**, 045802 (2012).
[17] A. Kara, H. Enriquez, A. P. Seitsonen, L. L. Y. Voon, S. Vizzini, B. Aufray, and H. Oughaddou, Surf. Sci. Rep. **67**, 1 (2012).
[18] P. D. Padova, P. Perfetti, B. Olivieri, C. Quaresima, C. Ottaviani, and G. L. Lay, J. Phys.: Condens. Matter **24**, 223001 (2012).
[19] B. Feng, Z. Ding, S. Meng, Y. Yao, X. He, P. Cheng, L. Chen, and K. Wu, Nano Lett. **12**, 3507 (2012).
[20] L. Chen, C.-C. Liu, B. Feng, X. He, P. Cheng, Z. Ding, S. Meng, Y. Yao, and K. Wu, Phys. Rev. Lett. **109**, 056804 (2012).
[21] X.-T. An, Y.-Y. Zhang, J.-J. Liu, and S.-S. Li, Appl. Phys. Lett. **102**, 043113 (2013).
[22] M. Tahir, A. Manchon, K. Sabeeh, and U. Schwingenschlögl, Appl. Phys. Lett. **102**, 162412 (2013).
[23] C. J. Tabert and E. J. Nicol, Phys. Rev. B **87**, 235426 (2013).
[24] Y. Cai, C.-P. Chuu, C. M. Wei, and M. Y. Chou, Phys. Rev. B **88**, 245408 (2013).
[25] L. Meng, Y. Wang, L. Zhang, S. Du, R. Wu, L. Li, Y. Zhang, G. Li, H. Zhou, W. A. Hofer, and H.-J. Gao, Nano Lett. **13**, 685 (2013).
[26] V. Vargiamidis, P. Vasilopoulos, and G.-Q. Hai, J. Phys.: Condens. Matter **26**, 345303 (2014).
[27] T. Aizawa, S. Suehara, and S. Otani, J. Phys. Chem. C **118**, 23049 (2014).
[28] D. Chiappe, E. Scalise, E. Cinquanta, C. Grazianetti, B. van den Broek, M. Fanciulli, M. Houssa, and A. Molle, Adv. Mater. **26**, 2096 (2014).
[29] D. Jose and A. Datta, Acc. Chem. Res. **47**, 593 (2014).
[30] L. L. Y. Voon and G. Guzmán-Verri, MRS Bull. **39**, 366 (2014).
[31] Y. Yao, S. Y. Liu, and X. L. Lei, Phys. Rev. B **91**, 115411 (2015).
[32] L. Tao, E. Cinquanta, D. Chiappe, C. Grazianetti, M. Fanciulli, M. Dubey, A. Molle, and D. Akinwande, Nat. Nanotechnol. **10**, 227 (2015).
[33] A. Dimoulas, Microelectron. Eng. **131**, 68 (2015).

[34] M. Houssa, A. Dimoulas, and A. Molle, J. Phys.: Condens. Matter **27**, 253002 (2015).
[35] R. Friedlein and Y. Yamada-Takamura, J. Phys.: Condens. Matter **27**, 203201 (2015).
[36] C. Grazianetti, E. Cinquanta, and A. Molle, 2D Mater. **3**, 012001 (2016).
[37] T. P. Kaloni, G. Schreckenbach, M. S. Freund, and U. Schwingenschlögl, Phys. Status Solidi RRL **10**, 133 (2016).
[38] J. Zhao, H. Liu, Z. Yu, R. Quhe, S. Zhou, Y. Wang, C. C. Liu, H. Zhong, N. Han, J. Lu, *et al.*, Prog. Mater. Sci. **83**, 24 (2016).
[39] M. J. Spencer and T. Morishita, *Silicene: Structure, Properties and Applications* (Springer, Switzerland, 2016).
[40] B. I. Shklovskii and A. L. Efros, *Electronic Properties of Doped Semiconductors* (Springer-Verlag, Berlin, Heidelberg, GmbH, 1984).
[41] A. Gold, J. Serre, and A. Ghazali, Phys. Rev. B **37**, 4589 (1988).
[42] D. N. Quang and N. H. Tung, Phys. Status Solidi B **209**, 375 (1998).
[43] U. Pinsook, A. Thongnum, and V. Sa-yakanit, Appl. Phys. Lett. **102**, 162101 (2013).
[44] U. Ekenberg, Phys. Rev. B **30**, 3367 (1984).
[45] A. Ghazali, A. Gold, and J. Serre, Phys. Rev. B **39**, 3400 (1989).
[46] E. Economou, *Green's Functions in Quantum Physics*, Springer Series in Solid-State Sciences (Springer, Berlin, Heidelberg, 2006).
[47] V. Samathiyakanit, J. Phys. C **7**, 2849 (1974).
[48] V. Sa-yakanit, Phys. Rev. B **19**, 2266 (1979).
[49] V. Sa-yakanit and H. R. Glyde, Phys. Rev. B **22**, 6222 (1980).
[50] B. I. Halperin and M. Lax, Phys. Rev. **148**, 722 (1966).
[51] P. Van Mieghem, G. Borghs, and R. Mertens, Phys. Rev. B **44**, 12822 (1991).
[52] P. Van Mieghem, Rev. Mod. Phys. **64**, 755 (1992).
[53] S. John, M. Y. Chou, M. H. Cohen, and C. M. Soukoulis, Phys. Rev. B **37**, 6963 (1988).
[54] A. Ghazali and J. Serre, Phys. Rev. Lett. **48**, 886 (1982).
[55] J. Serre and A. Ghazali, Phys. Rev. B **28**, 4704 (1983).
[56] J. R. Klauder, Ann. Phys. (NY) **14**, 43 (1961).
[57] K.-C. Ng, J. Chem. Phys. **61**, 2680 (1974).
[58] L. Matthes, O. Pulci, and F. Bechstedt, New J. Phys. **16**, 105007 (2014).
[59] F. Zakerian and M. Berahman, Opt. Quantum Electron. **48**, 1 (2016).
[60] T. W. Appelquist, M. Bowick, D. Karabali, and L. C. R. Wijewardhana, Phys. Rev. D **33**, 3704 (1986).
[61] V. N. Kotov, V. M. Pereira, and B. Uchoa, Phys. Rev. B **78**, 075433 (2008).
[62] D. V. Khveshchenko, J. Phys.: Condens. Matter **21**, 075303 (2009).
[63] P. K. Pyatkovskiy, J. Phys.: Condens. Matter **21**, 025506 (2009).
[64] J.-N. Zhang, Phys. Scr. **83**, 035002 (2011).
[65] H.-R. Chang, J. Zhou, H. Zhang, and Y. Yao, Phys. Rev. B **89**, 201411 (2014).
[66] C. J. Tabert and E. J. Nicol, Phys. Rev. B **89**, 195410 (2014).
[67] B. Van Duppen, P. Vasilopoulos, and F. M. Peeters, Phys. Rev. B **90**, 035142 (2014).
[68] P. C. Martin and J. Schwinger, Phys. Rev. **115**, 1342 (1959).
[69] R. Kubo, J. Phys. Soc. Jpn. **12**, 570 (1957).